Enabling mMTC in Remote Areas: LoRaWAN and LEO Satellite Integration for Offshore Wind Farm Monitoring

Muhammad Asad Ullah, *Student Member, IEEE*, Konstantin Mikhaylov, *Senior Member, IEEE*, and Hirley Alves, *Member, IEEE*

***Abstract*—The offshore wind farms are gaining momentum due to their promise to offer sustainable energy with low pollution and greenhouse gas emission. However, despite all the immense technological progress of recent years, the operation in a harsh and hard-to-reach environment remains challenging. According to the reports, each offshore wind turbine requires five maintenance visits a year on average, and the cumulative repair costs constitute around 30% of the turbine's life-cycle expenditure. Motivated by the advancement of massive machine-type connectivity (mMTC) and satellite technologies, in this study, we investigate the potential of these to enable remote monitoring of the offshore wind farms. Specifically, the two alternative architectures are considered. The indirect architecture relies on using a local mMTC gateway (GW) with a backbone over a reliable communication channel (e.g., satellite or wire-based). The direct approach implies the transmission of the data by sensors on the wind turbines directly to the mMTC GW on the low-Earth-orbit satellite. The details of the system design, the alternative implementation strategies, and relevant pros, cons, and trade-offs are pin-pointed. Finally, we employ simulations using realistic deployment and traffic and advanced propagation and collision models to characterize these two approaches' feasibility and packet delivery probability numerically when implemented over LoRaWAN mMTC technology.**

***Index Terms*—LoRaWAN, massive machine-type connectivity (mMTC), monitoring, remote area, renewable, satellites, wind turbines, wireless sensor network.**

I. Introduction

A. Renewable Energy and Offshore Wind Power

THE recent decade has steered the focus of academia and industry toward enabling and supporting sustainable development and CO_2 emission reduction. The sustainable development goals declared by the United Nations stress the need for novel resource-efficient solutions to fight climate change and environmental degradation. On the regional scale, the European Green Deal drives the development of a sustainable economy, cutting the pollution and greenhouse gas emission, with the ultimate goal of making Europe climate neutral by 2050. The use of renewable energy sources (e.g., thermal, photovoltaics/sunlight, and the kinetic energy of wind and water) is commonly seen as the way to go.

The statistics [1] reveal that wind and hydropower accounted for two-thirds of the total electricity generated from renewable sources in the European Union (EU). On the global scale, the cumulative capacity of the wind power generators already installed exceeds 650.8 GW and continues to rise. Despite being more expensive to construct, offshore wind farms feature higher efficiency and face lower social resistance than their onshore counterparts. For these reasons, offshore wind power generation is expected to grow at a fast pace in the years to come.

The importance of offshore wind energy is illustrated well by the current state and the future development plans in this sector worldwide. The world's first offshore wind farm was built in 1991, 2 km away from the shore near the town of Vindeby in Denmark [2]. By February 2021, Denmark had already 6228 wind turbines, including 558 offshore, which cover the 47% electricity consumption. Norway has announced the plans to develop two new offshore wind turbine farms, named Utsira Nord and Sørlige Nordsjø II, of 1010 and 2591 km^2, respectively. Since January 2021, the license award process has started, and the cumulative installed capacity of these two farms is expected to reach 4.5 GW. In the U.K., offshore wind electricity generation capacity is expected to reach 40 GW in the next nine years. The government of the Republic of Korea has declared the target to grow the production of renewable energy from 8% to 20% with 12-GW offshore wind power, and California, USA, intends to raise renewable electricity to 60% by 2030.

B. Wind Farm Failures and Their Prevention

The papers [3]–[7] shed some light on the major reasons and consequences of the wind farm failures. Specifically, the statistics reveal that the average failure rate for an offshore wind turbine is about ten failures per turbine per year by the

Manuscript received March 8, 2021; revised June 16, 2021 and August 12, 2021; accepted September 3, 2021. Date of publication September 14, 2021; date of current version February 18, 2022. This work was supported by the Academy of Finland through the 6Genesis Flagship project under Grant 318927 and the MRAT-SafeDrone project under Grant 341111. Paper no. TII-21-1121. *(Corresponding author: Muhammad Asad Ullah.)*

The authors are with the Centre for Wireless Communications, University of Oulu, 90014 Oulu, Finland (e-mail: muhammad.asadullah@oulu.fi; konstantin.mikhaylov@oulu.fi; hirley.alves@oulu.fi).

Color versions of one or more figures in this article are available at https://doi.org/10.1109/TII.2021.3112386.

Digital Object Identifier 10.1109/TII.2021.3112386

third year of wind turbine's operation, with 80% of those being minor repairs (material cost below 1000 EUR), 17.5% major repairs (material cost below 10 000 EUR), and 2.5% major replacements (material cost above 10 000 EUR). Generator and gearbox failures make up 95% of all failures in the major replacement category [3]. The gearbox is one of the most vulnerable subsystems accounting for 20% of the maintenance breaks [4]. All in all, the costs of maintenance accumulate to nearly 30% of the total costs during the life cycle of an offshore wind turbine [5].

On average, five site visits per annum [6] for each turbine are required to keep the energy production stable. Of these, only one is scheduled and serves for a regular annual inspection of all the components and subsystems. The other unscheduled visits deal with versatile faults and breakdowns. The intelligent remote surveillance and monitoring systems and preemptive maintenance feature an excellent potential for preventing breakdowns, thus bringing down the operational costs and reducing the wind turbine's offline time due to failure [7]. A brief survey of the condition monitoring systems (CMSs), fault diagnostic techniques, and critical issues for wind turbines is given in [8]. Notably, research and development of wind turbine monitoring and fault detection solutions experienced a remarkable boost during recent years [9].

The monitoring and analysis of as much as 150–250 physical parameters are desired to optimize the performance and assess the structural integrity of a single wind turbine today [10]. Commercial CMSs primarily use wired communication to transmit sensor data, which implies routing-dedicated cables both inside a turbine and between turbines over the bottom of the sea. The collected data are further streamed into the supervisory control and data acquisition (SCADA) system, which acts as a cardiovascular system of the entire wind farm. To effectively use the available bandwidth of the communication channel and the storage capabilities, the sensors' data are typically aggregated over a 10-min period [11].

C. Our Contributions

The contribution of this study is twofold.

1) First, we propose two novel approaches enabling wireless collection of sensor data from the offshore wind turbines. Both proposed solutions imply using state-of-the-art machine-type connectivity (MTC) solutions, namely, LoRaWAN technology. In the former case, data are collected by a local gateway (GW), located on one of the turbines, which further streams them through a wired or wireless link. In the latter case, data are collected by a satellite-based non-terrestrial GW(s). Notably, our obtained results can be further generalized for other applications and use cases, and other radio access technologies.
2) Second, we use simulations to analyze these two approaches' performance, highlighting their pros, cons, and notable trends. Importantly, we base our simulations on: a) real-life wind farms and wind turbine positions; b) traffic models and sensor deployments specific for wind turbine monitoring; c) characteristics of the communication devices equivalent to the ones currently available on the market; d) accounting for line-of-sight (LOS) blockage by the turbines; e) optimizing the position of the local GW; and f) employing experiment-based radio propagation and advanced collision models.

D. Article Structure

The rest of this article is structured as follows. Section II briefly presents the background of wireless monitoring of turbines, massive machine-type connectivity (mMTC), and satellite technologies. Section III introduces the indirect and direct LoRaWAN-satellite convergence architectures and pinpoints the associated tradeoffs. System model implications for our simulations and key parameters are listed in Section IV. Next, we report the illustrative numerical results in Section V. Finally, Section VI concludes this article.

II. Technical Background and Recent Developments

A. Wireless Monitoring in Wind Farms

The typical wind farm CMSs comprise complex communication infrastructure with a dedicated wired network spanning over a long distance that does not support real-time monitoring and failure prediction due to low frequency of updates [11]. Moreover, despite being costly, underwater cables carrying the sensors' data are also vulnerable to damage and are hard to repair. To address this challenge, several scholars suggested solutions based on wireless sensor networks for monitoring the health of offshore wind turbine components: blades, hub, tower, and nacelle.

Following are a few practical examples.

1) Ahmed *et al.* [12] conceptualize the design of a wind farm communication network for collecting sensor data from components and subsystems of the turbines by utilizing ZigBee, WiFi, and WiMAX technologies. Specifically, they present a four-layer (wind farm, data acquisition, communication network, and application layers) model for the future cyber-physical wind energy system.
2) In [4], a wireless CMS based on the nRF24L01 radio transceiver module has been promoted to early detect the gearbox faults.
3) Cao *et al.* [13] introduce a mobile-edge-computing-driven unmanned aerial vehicle to visually inspect the wind turbines with an HD camera and report the data through a satellite.

The introduction of mMTC (note that throughout this article, we use term mMTC to denote the versatile connectivity solutions intended for masses of machines with limited traffic requirements, whether these technologies are coming from 3GPP or not), and the low-power wide-area network (LPWAN)-grade technologies offering cost and energy-efficient solutions for small data transfers from different machines, feature a great potential to revolutionize the landscape of the Internet of Things (IoT) applications. Among notable features, which make these technologies perspective for remote monitoring, is their coverage, which can reach units to dozens of kilometers, depending

on the environment. This allows a single mMTC GW to cover the whole wind farm. The use of mMTC and, specifically, LoRaWAN for on-shore wind turbine sensor data collection has recently been conceptualized and demonstrated in-field in [14]. However, due to the typical absence of the conventional communication infrastructure, offshore wind farm monitoring (and monitoring in a remote area in general) introduces another challenge: the transfer of the already collected sensor data. We see two major ways of how this challenge can be approached. The former implies provisioning to the local GW with some form of backbone connectivity (e.g., a satellite channel). The alternative is deploying the new types of non-terrestrial infrastructure (e.g., satellites, high-altitude balloons, or drones), providing connectivity in the remote areas. In this study, we investigate the potential of both these approaches. Therefore, in the following two sections, we concisely discuss the enabler technologies' technical background—the LPWAN, in particular, LoRaWAN, and satellite technologies.

B. mMTC Technologies and LoRaWAN

Driven by global digitization, mMTC technologies answer the need to provide massive ubiquitous wireless connectivity while featuring very low energy consumption. LPWANs represent a group of technologies within the mMTC, which offer long range (LoRa), massive connectivity, and scalability subject to low energy consumption. In this family, the three promising technologies, namely, LoRaWAN, Sigfox, and NB-IoT, dominate the market. LoRaWAN and Sigfox both use sub-gigahertz unlicensed industrial, scientific, and medical (ISM) frequency plans depending on the geographical regions (around 868 MHz in the EU and 915 MHz in the USA/Asia). NB-IoT, developed within 3GPP (Rel. 13), operates in the licensed frequency band and is based on substantially revised and simplified Long-Term Evolution mechanisms. Note that neither Sigfox nor LoRaWAN ties the sensors [termed end-devices (EDs)] to a specific GW. Instead, each GW sends all the received packets to a central entity (denoted network server (NS) for LoRaWAN), which takes care of their further processing. Of these three technologies, only LoRaWAN GWs are readily commercially available, allowing deployment of the so-called private networks, which are managed not by dedicated telecommunication service providers. A private person or a company can easily get LoRaWAN GWs from the market to deploy a private network, which is not the case for Sigfox and NB-IoT. In the specific case of an offshore wind farm, this can be the farm's operator deploying and controlling the network, which makes this technology especially well suited.

LoRaWAN technical solution is primarily built on top of the proprietary LoRa modulation—a variant of chirp spread spectrum modulation. The spreading factor (SF) of the signal can be varied between SF7, SF8, . . . , SF12, thus trading the time on air (ToA) for the maximum radio coverage [15]. Notably, signals from different SFs are quasi-orthogonal, allowing concurrent decoding at the GWs. The node's SF allocation can be made statically or dynamically by the network or the node itself. For uplink transmissions, the basic (i.e., class A) nodes randomly select one supported by the network channel and send their data to the GWs. Two opportunities for transferring the downlink data are provided following each uplink transmission. Notably, practical air-to-ground trials have shown a LoRaWAN GW's possibility to successfully receive a packet from the distance of 832 km using 25-mW [16] transmit power.

C. Satellite Technologies as Enabler for Remote MTC

The satellites systems are classified into low Earth orbit (LEO, altitude below 2000 km), medium Earth orbit (2000–10 000 km), and geostationary orbit (GEO, 35 000 km) based on the orbit altitudes. Compared to the two other classes, LEO satellites enjoy the lowest propagation attenuation and delay for their transmissions. However, this is achieved at a cost of high orbital velocity, reaching about 27 000 km/h, and resulting in a mere 10-min time when a spot on the ground is within the LOS of an LEO satellite. Therefore, to ensure noninterrupted coverage, a constellation of multiple satellites is required. For example, Iridium constellation comprises 66 operational satellites distributed over six circular orbital planes with planar separation of 31.6° and having an altitude of approximately 780 km above the ground level.

In the past few years, global LEO marketplace has experienced significant growth. As an impressive milestone, as of August 2, 2021 [17], there are 3328 active LEO satellites (increasing by 126.70% from September 30, 2019). The development of the CubeSat concept, delivering a uniform form factor for satellites, thus reducing the launch and development costs and lowering the barrier to enter the market, has become one of the drivers beyond this. The potential of using the satellites for backhauling mMTC data transfers has already been suggested [18]. Specifically, smart city infrastructure is presented in [19], where mMTC nodes transfer their data to a GW, which streams them further over a satellite modem. A similar approach for offshore oil monitoring based on LoRaWAN technology has been trialed in [20].

However, recently, the possibility of enabling direct communication between mMTC devices and a satellite has been realized. The International Maritime Satellite Organization and MediaTek have reported successful satellite and cellular networks tests between a ground NB-IoT node and a GEO satellite [21]. The initial experiments on sending LoRa-modulated signals to and from satellites using reasonably low transmit power, reported in [22], have also proved the feasibility of this concept. Specifically, Lacuna Space has launched four satellites with LoRaWAN GWs in space as of November 9, 2020. The space GW is intended to receive and deliver to Earth the data collected from the low power LoRaWAN nodes deployed in hard-to-reach areas [23]. Notably, the recent laboratory tests and outdoor experiments reveal that mMTC-based LoRa technology has high immunity against the Doppler effect for satellite communication with the orbital altitude of 550 km [24]. To answer the same question, in [25], Fernandez *et al.* assess the Doppler effect at 868 and 915 MHz, which gives the maximum frequency shift of 22.56 and 23.78 kHz, respectively. Considering the channel separation of 200 and 125-kHz signal bandwidth commonly employed for LoRaWAN, the technology can be used with minimal

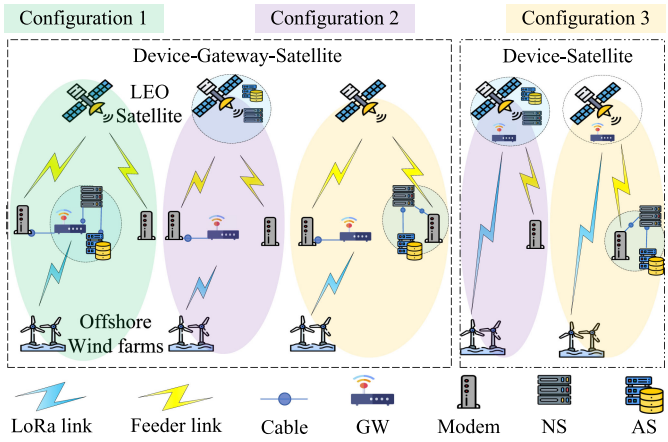

Fig. 1. System model of direct (right) and indirect (left) LoRaWAN-based LEO satellite integration with different network (NS) and application server (AS) placement alternatives. Notably, the three illustrated configurations (differentiated by green, purple, and yellow color) are alternative, and only one can be implemented at a time.

changes. Moreover, the study also assesses the capabilities of using LoRa for satellite-to-Earth communication and presents four different satellite and ground terminal configurations with motivation to enable seamless mMTC connectivity for hard-to-reach areas [25].

The paper [26] discusses the state of the art of network topologies for LEO-satellite-based LoRa constellation and possible future research directions. Furthermore, Fraire *et al.* [27] suggest a design of a quasi-optimal topology for sparse satellite constellations and results confirm that only nine LoRa-compatible LEO satellite are sufficient to provide global LoRaWAN coverage.

III. LoRaWAN-Satellite Convergence and the Alternative Implementation Strategies

In this section, we dive deeper into how the convergence of LoRaWAN and satellite can be enabled. Note that somewhat similar architectures can be considered for the other mMTC technologies. Specifically, we sketch the two possible communication architectures and point out relevant practical constraints and tradeoffs associated with these implementation strategies, which are illustrated in Fig. 1.

A. Indirect: mMTC Device Gateway Satellite

The hybrid "indirect" mMTC-satellite network architecture comprises two elements: the ground and the air segments. In the ground segment, sensors transmit the monitored data to a local GW(s) over an mMTC (e.g., LoRaWAN) technology. The GWs stream the data further over the feeder link to the satellite. Notably, this architecture enables three alternative options to distribute the LoRaWAN network elements and management entities.

1) NS/AS are located before the satellite link.
2) NS/AS are located after the satellite link.
3) NS/AS are located within the satellite constellation.

Each of these alternatives has pros and cons. Specifically, option 1 allows benefiting from aggregation and compression, thus reducing traffic through the satellite. The downside is a more sophisticated and costly on-ground infrastructure, which can become a bottleneck performance and dependabilitywise. Option 2 enables to simplify the local GW's design by moving all the burden of network management to the ground component beyond the satellite link. This approach's downsides are increased traffic through the satellite channel and more stringent latency and reliability requirements. Finally, option 3 is a compromise between the two others. Despite being a potentially perspective approach for implementing monitoring of a static offshore wind farm, the indirect architecture is less suitable for the applications implying mobility. The freely floating sensors in the sea represent just one of the illustrative examples.

B. Direct: mMTC Device Satellite

The "direct" architecture empowers each node to directly transmit its data to a GW in space without relying on any local GWs. Furthermore, the satellite's elevation enables to increase the probability of LOS for the sensors not obstructed by obstacles around. Notably, the conventional mMTC technologies' sub-gigahertz frequency bands do not suffer from the strong attenuation caused by atmospheric gases, rain droplets, and fog. The absence of the handovers, minimal signaling, and possibility of data reception by any GW implemented in, e.g., LoRaWAN and Sigfox, make such technologies very promising for the direct architecture.

However, there are two notable challenges associated with this approach. The first one is the ultralong (hundreds to thousands of kilometers) communication distance between a node and a satellite. The second one is the network scalability issue and, specifically, the possibility of handling myriads of small-data transfers. Both these issues can be approached by equipping the mMTC GW satellites with efficient multibeam high-gain directive antennas. This is also worth noting that the longer communication distances cause longer delays (and, notably, their variation), which may result in the need to modify some of the protocol parameters and constants (e.g., the receive window delays and duration in the case of LoRaWAN).

IV. System Model and Implications

To investigate the feasibility and shed some light on the potential performance and the tradeoffs specific to the two alternative implementation strategies discussed in the previous section, we conducted extensive simulations considering the offshore wind farm application. However, these network architectures could be a viable solution for the other applications, which lack wireless communication infrastructure and coverage (e.g., mMTC applications—in sea, very remote areas, and smart farming in desert). The key models and implications for these are detailed in the following subsections.

A. Wind Farm Model and Sensor Distribution

As reference for our simulations, we intentionally selected the most challenging offshore wind generation deployments near Denmark's shore: 1) featuring the highest number of windmills; 2) realizing two interesting deployment layouts, i.e., the grid

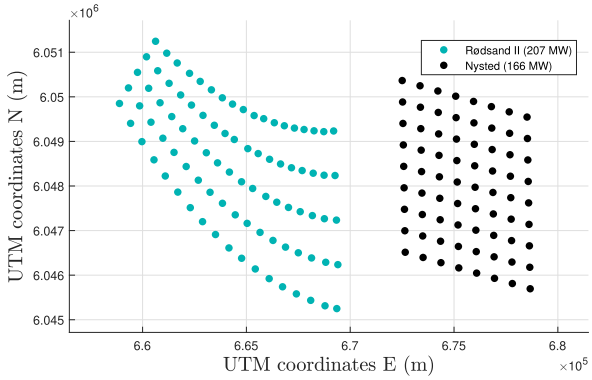

Fig. 2. Layout of 162 operational turbines in Rødsand II (left) and Nysted (right) offshore wind farms with rated capacities of 207 and 166 MW, respectively.

TABLE I
KEY APPLICATION PARAMETERS [10], [11], [28]

Parameters	Requirements
Application payload (P_L)	10 bytes
Update rate (D)	600 s
Data transmissions	Unacknowledged
Traffic pattern	Periodic
No. of Wind turbine (M)	162
No. of Gateway	1
Hub height	69 meters
Nacelle radius (R_n)	3.4 meters
Nodes/wind turbine (S)	50
Total nodes (N)	8100
Nodes deployment	Uniform
Nysted Layout	Grid
Rødsand II Layout	Curved polygon

and a curved polygon[1]; 3) with availability of the windmills coordinates data; and 4) extensively used as a reference in literature. Out target deployment is a combination of the two wind farms, named Nysted and Rødsand II, as illustrated in Fig. 2. The Nysted farm (right part of Fig. 2) was deployed first and comprises 72 Siemens operational units, which are placed in 8 (East–West) × 9 (North–South) grid with a spacing of $10.5D$ (East–West) and $5.8D$ (North–South), where D is the rotor diameter. In 2010, the deployment was extended with 90 additional turbines in about 34-km^2 area named Rødsand II (left part of Fig. 2). The total number of the wind turbines in both farms is $M = 162$, and the coordinates (obtained from interactive maps of the Danish Energy Agency [28]) for a W_j turbine we denote as $C_j = [x_j, y_j]$, where x_j and y_j represent geographic Cartesian coordinates toward East and North, respectively, for a given wind generator $j = 1, 2, \ldots, M$.

Based on the results and architectures presented in [10], we imply that each turbine is equipped with $S = 50$ sensor nodes, each monitoring five parameters. Thus, the farm as a whole composes $N = M \times S$ nodes. Furthermore, we approximate each wind turbine's surface with a circle of 3.4-m radius (which corresponds to the nacelle dimension of a 2.3-MW Siemens offshore wind turbine) and imply that the sensor nodes are uniformly distributed around the nacelle. The key application parameters and requirements of simulated scenario are listed in Table I.

B. Data Traffic Model

We consider that sensed parameters are encoded into two data bytes each, yielding a 10-byte payload. A single-application-layer payload containing all five measured parameters is encapsulated into a conventionally formatted LoRaWAN packet. Following the commercially available CMS and SCADA systems [10], [11], we imply each node broadcasts the uplink packets with the period of $D = 600$ s. The on-air time for a single uplink transmission equals ToA $= \{61.69, 370.68, 1482.75\}$ ms for SF7, SF10, and SF12, respectively. Furthermore, we imply that the start time of the first uplink packet for each node is random and uniformly distributed between 0 and D, and denoted $t_{Ni} = U(0, D)$. Under these implications and considering the simulation time of 1 h (3600 s), the node N_i starts transmission of its packets at $\tau_{Ni,k} = t_{Ni} + kD$ and occupies a radio channel for the interval $[\tau_{Ni,k}; \tau_{Ni,k} + \text{ToA}]$, where $k = 0 \ldots \frac{\Delta}{D} - 1$ and Δ denotes simulation duration.

C. LoRaWAN Parameters and Configurations

Our key implications about the LoRaWAN network configuration are as follows: (i) we consider a network deployed in the 868-MHz ISM band under EU regional restrictions; (ii) EDs randomly select one of the eight configured frequency channels for transmissions; (iii) all nodes use the same LoRaWAN SF and same (maximum allowed) transmit power, and no adaptive data rate (ADR) is present due to mobility of satellite and lack of resources for downlink communication on a satellite; (iv) for a preselected network, all nodes are preconfigured with needed parameters and security credentials (e.g., DevAddr, NwkSKey, and AppSKey are flashed to the node's memory before it is deployed) and use activation by personalization; (v) we imply that all uplink transmissions are nonacknowledged; (vi) we imply no downlink application traffic; and (vii) to make the comparison fair, we further limit to only single GW for each of the considered architectures—indirect and direct. The implications (v) and (vi) are primarily due to the fact that our target use case does not imply any obligatory down-going traffic. Also, we mind the limited time–frequency resources of a satellite-based LoRaWAN GW for downlink and the potential of downlink traffic negatively affecting the network performance in LoRaWAN, which has been shown in the literature [36], [37]. Note that the implementation of downlink LoRaWAN traffic from a satellite-based GW would likely introduce novel technical challenges. One of these is handling of much higher (i.e., millisecond order) one-way propagation delays and their variation due to the change of distance between a device and a satellite-based GW. Note that the packet report period of ten minutes complies with the duty cycle

[1]OSPAR ODMIS, OSPAR Offshore Renewable Energy Developments—2016. [Online]. Available: https://odims.ospar.org/layers/geonode:ospar_offshore_renewables_2016_01_001

restrictions imposed on LoRaWAN in the EU. Also, this is worth noting that each node in the network must be configured with unique session keys and feature a mechanism preventing their reading to ensure security and prevent the widespread breach if a single node is compromised. In the case, a device has to be replaced; preferably, a new set of key should be configured.

D. Channel Models

We imply that in the absence of interference, a GW successfully decodes the uplink packet if the instantaneous signal-to-noise ratio (SNR) for the received signal is higher than the demodulator's SF-specific SNR threshold equal to $D_{\text{SNR}} = \{-6, -15, -20\}$ dB [32] for SF7, SF10, and SF12, respectively. The probability of the correct packet reception is denoted as

$$P_{\text{SNR}}(d_{T,n}) = \mathbb{P}\left[\frac{P_{tx} G_t G_r \text{PL}(d_{T,n}, \sigma, \gamma)|h|^2}{\sigma_w^2} \geq D_{\text{SNR}}\right] \quad (1)$$

where $\sigma_w^2 = -174 + NF + 10\log_{10}(B)$ dBm is variance of the additive white Gaussian noise, $d_{T,n}$ is the distance between the node and the GW, $NF = 6$ dB is LoRaWAN GW receiver's design architecture noise figure, G_t is the node's omnidirectional antenna gain which we imply equal 2.15 dBi (i.e., a half-wavelength dipole), and G_r is the directive antenna gain of the each beam generated by the satellite. Based on [25] and [33], we consider $G_r = 6.5$ dBi for the omnidirectional antenna of local GW in indirect implementation, and the two different options (i.e., "advanced" and "basic" antennas) $G_r = \{10, 22.6\}$ dBi for aerial GW in the direct architecture. In space segment, the key design requirements of the L-band directive antenna include lightweight structure, high efficiency in space environment, and the ability to handle multiple-beam operation simultaneously. The channel coefficient (h) accounts for the nature of fading (i.e., Rayleigh or Rician) and is expressed as

$$h = \sqrt{\frac{K}{K+1}} h_{\text{LOS}} + \sqrt{\frac{1}{K+1}} h_{\text{NLOS}} \quad (2)$$

where K is the Rician factor. To account for the propagation losses, we opted for the classical log-distance path-loss model given by

$$\text{PL} = \text{PL}_0 + 10\log_{10}\gamma \frac{d_{T,n}}{d_0} + X_g \quad (3)$$

where PL_0 is the free space path loss at d_0 reference distance, γ is the path-loss exponent, $d_{T,n}$ is the path length between the transmitter and the receiver, and $X_g \sim \mathcal{N}(0, \sigma^2)$ is the zero-mean Gaussian random variable with standard deviation (STD) σ, which accounts for the shadowing.

1) Signal Propagation for Indirect Architecture: For indirect architecture, we distinguish two different cases: the LOS and the non-line-of-sight (NLOS) propagation. As Fig. 2 illustrates, the turbines are often installed in a regular grid, which increases the chance that turbines located between the GW (located on a turbine) and the sensors placed on another turbine may block the LOS, as illustrated in Fig. 3.[2]

[2]For the sake of clarity, Fig. 3 illustrates only single blocking turbine. In our models, we also consider cases of multiple turbines blocking LOS.

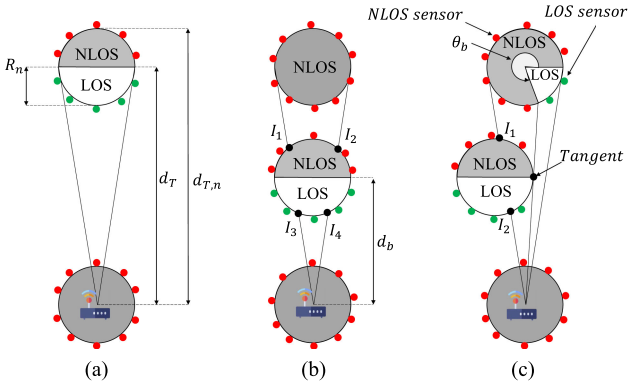

Fig. 3. LOS, NLOS, and partially obstructed LOS scenarios (illustration). (a) LOS case. (b) NLOS case. (c) Partially shadowed.

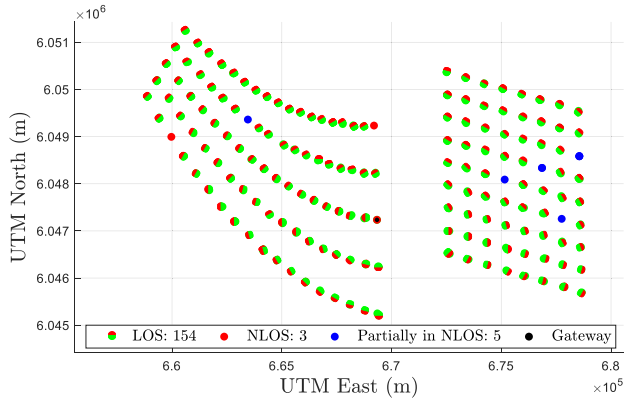

Fig. 4. Selected GW location for indirect architecture and LOS status of the turbines for it.

Assume that the GW's coordinates are $C_G = [x_G, y_G]$, and $C_T = [x_T, y_T]$ are the coordinates of target windmill. Considering the nacelle radius $R_n = 3.4$ m, $x_{T,n} = x_T + \frac{R_n \cos(\theta_n)}{2}$ and $y_{T,n} = y_T + \frac{R_n \sin(\theta_n)}{2}$ are the coordinate of the nth node at the target wind turbine, where $n = 1, 2, \ldots, S$ and $\theta_n = \frac{2\pi}{S} \times n$. Then, the LOS status of the node is defined as

$$f(I) = \begin{cases} \text{LOS}, & d_{T,n} \leq d_T \quad \text{and} \quad I < 2 \\ \text{NLOS}, & d_{T,n} > d_T \quad \text{and} \quad I < 2 \\ \text{NLOS}, & d_{T,n} > d_b \quad \text{and} \quad I = 4 \\ \text{LOS}, & \theta_b < \theta_n \quad \text{and} \quad 2 <= I < 4 \end{cases} \quad (4)$$

where I is the number of intersections of the tangent lines to the target turbine originating from the GW position and the obstructing turbines, and d_T and $d_{T,n}$ denote the Euclidean distance from the GW tangent point(s) and the target node, respectively. Furthermore, d_b denotes the distance between the center of the blocking windmill and the GW, and θ_b is illustrated in Fig. 3. To determine the position of the local GW, we have used the brute-force method to locate a turbine featuring the minimum number of NLOS nodes and the minimum average distance of all nodes. The resulting location of the GW and the LOS status of other turbines are depicted in Fig. 4, where the green, red, and blue colors reflect visibility relation between target windmill and

the local GW as LOS, NLOS and partially blocked, respectively. After determining the LOS status of each node, for the ones located in LOS, we imply that their channel follows the Rician distribution with $K = 4$ dB, $\sigma = 0.1$ dB, and $\gamma = 2$ [30]. For the case of NLOS, we imply that the channel undergoes Rayleigh fading. To the best of the authors' knowledge, there is no study available that reports the measurement of channel characteristics in offshore wind farm scenario. Based on the results of the empirical measurements reported in [29] and [31], we assume the most appropriate value as $K = 0$, $\sigma = 4$ dB, and $\gamma = 3$. Without loss of generality, we also imply that from the local GW, the collected data are delivered through a reliable communication channel (e.g., satellite-based).

2) Signal Propagation for Direct Architecture: For the direct architecture, we imply that the LOS passes directly above the wind farm, and that for each elevation angle, the antenna beam is centered at the center of the wind farm. Following the basic orbital geometry, the slant distance between a specific ground node and the satellite at a given elevation angle (E) is

$$d_{T,n} = R\left[\sqrt{\left(\frac{H+R}{R}\right)^2 - \cos^2(E)} - \sin(E)\right] \quad (5)$$

where $R = 6378$ km is the radius of Earth, $H = 780$ km is the orbital height of the satellite, and E is defined as

$$E = \sin^{-1}\left(\frac{H\,(H+2R) - d_{T,n}^2}{2d_{T,n}R}\right). \quad (6)$$

We imply that the farm remains in the satellite's sight as long as E stays above 10°. When modeling the channel between the nodes and the satellite, we consider the time-varying characteristics of the fading effect with a dynamic Rician factor (K), which depends on E [35], as illustrated in Fig. 8. Benefiting from the high altitude of the satellite, we imply that the communication is always LOS, and thus, $\sigma = 0.1$ dB and $\gamma = 2$ [30].

E. Interference Models

The recent empirical and analytical studies have demonstrated the presence of the capture effect [32] for LoRa signals, which enables a receiver to demodulate the stronger signal under the interference from the weaker ones. To account for the co-SF interference, we imply the packet collision model similar to [38]. Mathematically, the LoRaWAN success probability accounting for the same-channel same-SF interference can be defined as

$$P_{\text{SIR}}(d_{T,n}) = \mathbb{P}\left[\frac{P_{tx}G_tG_r\text{PL}(d_{T,n},\sigma,\gamma)|h|^2}{\sum P_{tx}G_tG_r\text{PL}(d_i,\sigma_i,\gamma_i)|h_i|^2} \geq \delta\right]. \quad (7)$$

where i denotes the interfering signal and $\delta = 6$ dB is the power threshold. The characteristics of the physical channel (e.g., d_i, σ_i, γ_i, and h_i) and the path loss PL for the interfering nodes are defined based on their LOS/NLOS status, as discussed in Section IV-D. Furthermore, we consider that there is no interchannel and inter-SF interference between the transmissions carried in the different frequency channels and different SFs, respectively.

TABLE II
KEY MONTE CARLO SIMULATION PARAMETERS

Parameters	Values
Carrier frequency (f_C)	868 MHz
Bandwidth (B)	125 kHz
Channels	8
Transmit power (P_{tx})	14 dBm
Noise power ($\mathcal{N}$)	-117 dBm
Spreading factor (SF)	7, 10, 12
Elevation angles (E)	$10° \leq E \leq 90°$
Rician Factor (K) [35]	$1.24 \leq K \leq 25.11$
Orbital height (H)	780 km
Earth Radius (R)	6378 km

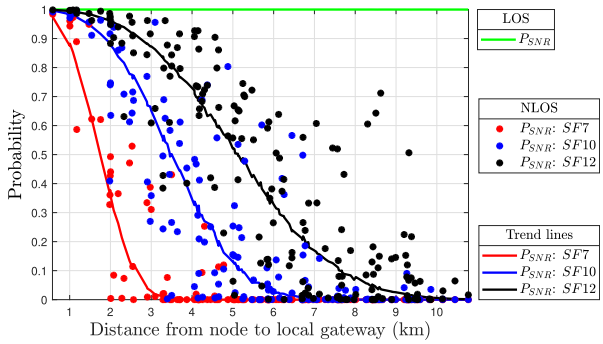

Fig. 5. Average P_{SNR} for indirect architecture for nodes in LOS/NLOS.

F. Cumulative Probability of Packet Delivery

The overall probability of successful packet delivery is product of $P_{\text{SNR}}(d_{T,n})$ and $P_{\text{SIR}}(d_{T,n})$, i.e.,

$$P_S(d_{T,n}) = P_{\text{SIR}}(d_{T,n})\,P_{\text{SNR}}(d_{T,n}). \quad (8)$$

V. NUMERICAL RESULTS

To analyze the performance of the two satellite-based mMTC architectures for offshore wind farm monitoring, we carried out the analysis using the specially developed MATLAB-based Monte Carlo simulator models (available from GitHub via [39]) featuring: 1) the offshore wind farm geospatial data; 2) the designed algorithm to determine the LOS status of node; 3) algorithm to optimize the location of the local GW; and 4) the evaluation of channel models. Each point presented on the chart is the average over 10^5 iterations' distributions unless stated otherwise. The key parameters of our model are listed in Table II.

A. Insights Into the Performance of Indirect Architecture

Fig. 5 depicts the average P_{SNR} for LOS and NLOS (a single realization and trends) nodes as a function of the distance between the local GW and a node. One can see that for LOS, P_{SNR} stays above 99.9% for all the SFs, while for NLOS, P_{SNR} experiences strong fluctuations and vastly decreases with the increase of the distance. When the distance between the node and the GW exceeds 8 km even using SF12, packet reception probability drops below 0.1.

Fig. 6 shows the average P_{SIR} for nodes in LOS and NLOS. Also, as the reference and to cross-validate the correctness of the

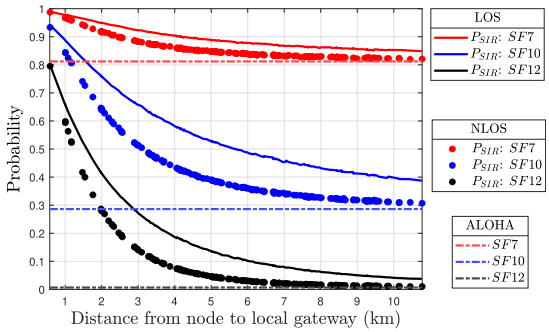

Fig. 6. Average P_{SIR} for indirect architecture for nodes in LOS/NLOS.

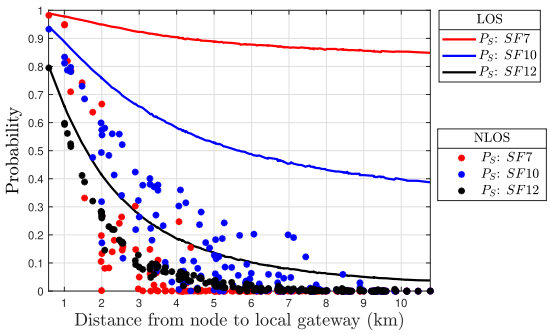

Fig. 7. Average overall success probability P_S for indirect architecture.

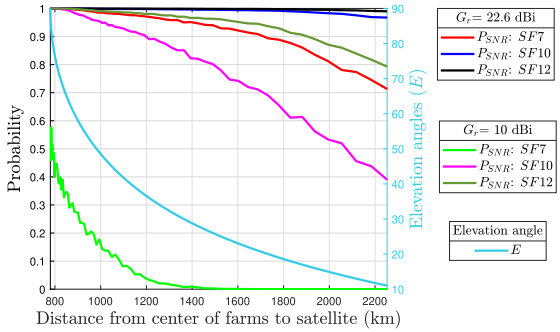

Fig. 8. Average P_{SNR} for direct architecture $G_r = \{10, 22.6\}$ dBi.

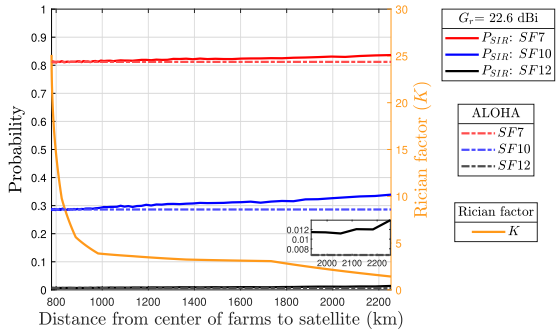

Fig. 9. Average P_{SIR} for direct architecture $G_r = 22.6$ dBi.

developed Monte Carlo simulator and establish the reference to the previous studies, we plot the analytical lines for probability of packet delivery for multifrequency-channel unslotted ALOHA calculated using $P_{\text{ALOHA}} = \exp(-\alpha_t \alpha_f \lambda_{tf})$, where λ_{tf} is the traffic load, $\alpha_t = 2$, and $\alpha_f = 1$ (refer to [34] for details). Note that the simulator also accounts for the influence of shadowing, propagation, capture effect, Rician, and Rayleigh fading, which are not accounted for by the analytic model of ALOHA.

One can see that the SF selection, directly related to the on-air time of the packet, strongly affects P_{SIR}. For SF7, the average P_{SIR} stays above 0.8. Note that with the decrease of the distance between the GW and a node, P_{SIR} increases due to capture effect, which is also the key reason for the difference in the performance of the nodes located in LOS and NLOS. Notice that P_{ALOHA} performs close to the lower bound of P_{SIR} for NLOS nodes.

Finally, Fig. 7 depicts the overall success probability for indirect architecture. Our results reveal that neither SF allows efficient data collection. SF7 works well for the nodes in LOS, but for NLOS ones, the increase of attenuation results in a vast decrease in the probability of successful packet delivery. SF12, despite allowing for the maximum communication distance, suffers from interference. SF10 provides a compromise, even though the overall performance stays low.

B. Insights Into the Performance of Direct Architecture

Fig. 8 reveals P_{SNR} for different receiving antenna gains. One can see that if the satellite's antenna gain is 10 dBi (typical for CubeSats), only the use of SF10 and SF12 enables a node to reach GW. However, with the increase of the gain to 22.6 dBi (antenna gain of Iridium satellites), P_{SNR} increases from 38.9% to 96.7% for SF10 at the maximum distance. When using SF7 and implying 10-dBi satellite antenna gain, the probability of successful packet delivery when the satellite is located at the closest point is about 0.6 and vastly decreases once the distance between the satellite and the farm increases. For 22.6-dBi antenna gain and implying use of SF7, even at the maximum distance, P_{SNR} stays above 71.3%. For reference, the elevation angle's dependence on the distance is plotted on the axis on the right in the chart.

P_{SIR} and reference lines for ALOHA, implying a satellite antenna gain of 22.6 dBi, are presented in Fig. 9. One can note that the probability obtained with simulation is slightly higher than that determined analytically for ALOHA. Interestingly, with the increase in the distance between the farm and the satellite (and the decrease of the elevation angle), P_{SIR} increases. This counterintuitive result is caused by the capture effect—with the decrease of the elevation angle, the difference between individual nodes' channel budgets increases, thus making the capture effect's occurrence more probable. Note that the second axis is used to illustrate the Rician factor as a function of distance.

Finally, Fig. 10 plots the overall success probability [given by (8)] for direct architecture. One can see that for SF7, P_S stays above 0.6 at all distances. When configured with SF10, the overall probability is close to 0.3 and increases with the increase in the distance due to the capture effect. Finally, the chance of packet delivery from the network configured with SF12 is meager.

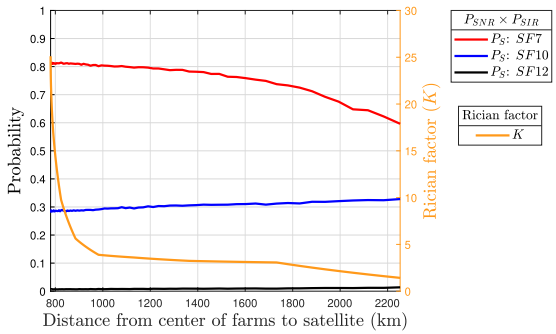

Fig. 10. Average overall success probability P_S of direct architecture for $G_r = 22.6$ dBi.

TABLE III
COMPARISON OF OVERALL SUCCESS PROBABILITIES P_S

Implementation	SF7	SF10	SF12
Indirect architecture	0.4628	0.3320	0.1173
STD (Indirect architecture)	0.4354	0.2695	0.1613
Direct architecture	0.7855	0.2964	0.0080
STD (Direct architecture)	0.0463	0.0121	0.0016

C. Comparison

Table III summarizes the average results of 10^5 iterations and compares the average and STD of P_S for the indirect and direct architectures. This can be seen that when operating with SF7, the direct architecture outperforms the indirect one, featuring 32.27% higher packet delivery. However, for higher SFs, the indirect approach enables higher packet delivery probability. It is also worth noting that the probability of successful packet delivery for individual nodes under direct architecture is quite similar. Note that the indirect architecture has higher STD due to the huge difference in the packet delivery probability of LOS and NLOS nodes, as illustrated in Fig. 7.

To summarize, our results reveal the feasibility of LEO satellite and LoRaWAN integration for the mMTC applications in remote areas. For direct architecture and LOS, one can see that the main reason behind performance degradation is the co-SF interference rather than the propagation, while for indirect architecture, the key challenge is NLOS propagation. Notably, we expect the results to be much better for the low-traffic applications with similar requirements.

VI. CONCLUSION

This article advocated the mMTC (LoRaWAN) and satellite integration for wireless condition monitoring of large-dense offshore wind farms. Our results showed that both of the considered architectures—indirect and direct—are potentially feasible. However, the probability of successful packet delivery remained relatively low in both cases. For the indirect case, the primary reason for this is the shadowing of the nodes by other turbines. For the direct case, this is caused by the great number of collisions and low variation of the channel budgets, not enabling to benefit from the capture effect.

All in all, serving 8100 devices reporting every 10 min remains a challenging task. Nonetheless, we are confident that the suggested approaches are perspective for the smaller wind farms or the other use cases implying fewer transmissions per time unit. However, for our analysis, we intentionally selected a very challenging scenario, featuring a great number of devices. Even today, many of the offshore farms have much less turbines, and thus, one could expect a much better performance. At the same time, there is much space for the future improvements.

Specifically, we consider the optimal allocation of different SFs to leverage their quasi-orthogonality to be a very prospective and challenging research direction for the future work. Similarly, we also consider this worth of investigating how to exploit the spatial diversity of the local GWs considering their optimal number along with the optimal deployment location as another open research challenge. The considered in this article traffic pattern is strictly periodic and matches that of the commercially available CMSs. As a consequence, if the transmissions of two or more nodes collide, this will likely happen also in the subsequent periods. Note that this does not affect directly the average packet delivery probability, which is used as a metric in this study. However, to increase the number of unique devices from which the data are received, one might consider introducing an additive random component to the transmission instants of each packet (e.g., likewise this is done in the advertising channel transmissions of Bluetooth Low Energy).

Similarly, the enablement of comfirmed and downlink traffic is a critical problem to be addressed in satellite-based LoRaWAN networks. The cumulative aggregated ACKs for multiple packets of multiple nodes can enable the confirmed uplink communication without significantly degrading the performance of the satellite-based LoRaWAN network. Moreover, the results can be further improved by enabling more frequency channels, exploiting the frequency hopping techniques, more directive antennas, or utilizing more sophisticated data encoding and aggregation schemes.

REFERENCES

[1] Eurostat, *Renewable Energy Statistics*. Accessed: Feb. 28, 2021. [Online]. Available: https://ec.europa.eu/eurostat
[2] European Parliament, *Offshore Wind Energy in Europe*. Accessed: Feb. 22, 2021. [Online]. Available: https://www.europarl.europa.eu
[3] J. Carroll, A. McDonald, and D. McMillan, "Failure rate, repair time and unscheduled O&M cost analysis of offshore wind turbines," *Wind Energy*, vol. 19, pp. 1107–1119, 2016.
[4] L. Lu, Y. He, Y. Ruan, and W. Yuan, "Wind Turbine Planetary Gearbox Condition Monitoring Method Based on Wireless Sensor and Deep Learning Approach," *IEEE Trans. Instrum. Meas.*, vol. 70, pp. 1–16, 2021, Art. no. 3503016.
[5] F. Besnard, K. Fischer, and L. B. Tjernberg, "A model for the optimization of the maintenance support organization for offshore wind farms," *IEEE Trans. Sustain. Energy*, vol. 4, no. 2, pp. 443–450, Apr. 2013.
[6] C. Röckmann *et al.*, "Operation and maintenance costs of offshore wind farms and potential multi-use platforms in the Dutch North Sea," in *Aquaculture Perspective of Multi-Use Sites in the Open Ocean*. Cham, Switzerland: Springer, 2017, pp. 97–113.
[7] X. T. Castellà, "Operations and maintenance costs for offshore wind farm analysis and strategies to reduce o&m costs," M.S. thesis, Dept. Ind. Eng., Nat. Taiwan Univ. Sci. Technol., Taipei, Taiwan, 2020.
[8] W. Qiao and D. Lu, "A survey on wind turbine condition monitoring and fault diagnosis—Part I: Components and subsystems," *IEEE Trans. Ind. Electron.*, vol. 62, no. 10, pp. 6536–6545, Oct. 2015.

[9] F. Qu, J. Liu, H. Zhu, and D. Zang, "Wind turbine condition monitoring based on assembled multidimensional membership functions using fuzzy inference system," *IEEE Trans. Ind. Informat.*, vol. 16, no. 6, pp. 4028–4037, Jun. 2020.

[10] Y. Wang, X. Ma, and P. Qian, "Wind turbine fault detection and identification through PCA-based optimal variable selection," *IEEE Trans. Sustain. Energy*, vol. 9, no. 4, pp. 1627–1635, Oct. 2018.

[11] Y. Vidal, F. Pozo, and C. Tutivén, "Wind turbine multi-fault detection and classification based on SCADA data," *Energies*, vol. 11, 2018, Art. no. 3018.

[12] M. A. Ahmed *et al.*, "Wireless network architecture for cyber physical wind energy system," *IEEE Access*, vol. 8, pp. 40180–40197, 2020.

[13] P. Cao, Y. Liu, C. Yang, S. Xie, and K. Xie, "MEC-Driven UAV-Enabled Routine Inspection Scheme in Wind Farm Under Wind Influence," *IEEE Access*, vol. 7, pp. 179252–179265, 2019, doi: 10.1109/ACCESS.2019.2958680.

[14] K. Mikhaylov, A. Moiz, A. Pouttu, J. M. Martín Rapún, and S. A. Gascon, "LoRa WAN for wind turbine monitoring: Prototype and practical deployment," in *Proc. 10th Int. Congr. Ultra Modern Telecommun. Control Syst. Workshops*, 2018, pp. 1–6.

[15] W. Ayoub, A. E. Samhat, F. Nouvel, M. Mroue, and J. Prévotet, "Internet of Mobile Things: Overview of LoRaWAN, DASH7, and NB-IoT in LPWANs standards and supported mobility," *IEEE Commun. Surv. Tut.*, vol. 21, no. 2, pp. 1561–1581, Apr.–Jun. 2019.

[16] *The Things network, LoRa World Record Broken: 832 km using 25 mW.* Accessed: Jun. 8, 2021.[Online]. Available: https://www.thethingsnetwork.org

[17] *Union of Concerned Scientists, UCS Satellite Database*. Accessed: Aug. 2, 2021. [Online]. Available: https://www.ucsusa.org/resources/satellite-database

[18] O. Kodheli *et al.*, "Satellite communications in the new space era: A survey and future challenges," *IEEE Commun. Surv. Tut.*, vol. 23, no. 1, pp. 70–109, First Quarter 2021

[19] R. Giuliano, F. Mazzenga, and A. Vizzarri, "Satellite-based capillary 5G-mMTC networks for environmental applications," *IEEE Trans. Aerosp. Electron. Syst.*, vol. 34, no. 10, pp. 40–48, Oct. 2019.

[20] *Satel Benelux*, "Satel Benelux has become distributor of Fleet LoRaWAN GW.," Accessed: Mar. 6, 2021. [Online]. https://www.satelbv.nl/products/industrial-telemetry-network/lorawan-gateway/

[21] Inmarsat, "Successful trial advances global 5G IoT communications.," Accessed: Jun. 8, 2021. [Online]. Available: https://corp.mediatek.com

[22] *The Things Network, LoRa transmission from low orbit satellite.* Accessed: Mar. 6, 2021. [Online]. Available: https://www.thethingsnetwork.org

[23] Lacuna Space, "Launch success: Lacuna space continues to grow IoT constellation with an equatorial satellite."Accessed: Jun. 8, 2021. [Online]. Available: https://lacuna.space/launch-success-with-an-equatorial-satellite/

[24] A. A. Doroshkin, A. M. Zadorozhny, O. N. Kus, V. Y. Prokopyev, and Y. M. Prokopyev, "Experimental study of LoRa modulation immunity to Doppler effect in CubeSat radio communications," *IEEE Access*, vol. 7, pp. 75721–75731, 2019.

[25] L. Fernandez, J. A. Ruiz-De-Azua, A. Calveras, and A. Camps, "Assessing LoRa for Satellite-to-Earth Communications Considering the Impact of Ionospheric Scintillation," *IEEE Access*, vol. 8, pp. 165570–165582, 2020, doi: 10.1109/ACCESS.2020.3022433.

[26] J. Fraire *et al.*, "Direct-to-satellite IoT—A survey of the state of the art and future research perspectives: Backhauling the IoT through LEO satellites," in *Proc. Ad-Hoc, Mobile, and Wireless Netw Conf.*, 2019, pp. 241–258.

[27] J. A. Fraire, S. Henn, F. Dovis, R. Garello, and G. Taricco, "Sparse satellite constellation design for LoRa based direct-to-satellite Internet of Things," in *Proc. IEEE Glob. Commun. Conf.*, Taipei, Taiwan, 2020, pp. 1–6.

[28] The Danish Energy Agency, "Wind power plants in Denmark.," Accessed: Mar. 3, 2021. [Online]. Available: https://ens.dk/service/statistik-data-noegletal-og-kort/interaktive-kort

[29] J. Wang *et al.*, "Wireless channel models for maritime communications," *IEEE Access*, vol. 6, pp. 68070–68088, 2018.

[30] X. Li *et al.*, "UAV-enabled accompanying coverage for hybrid satellite-UAV-terrestrial maritime communications," in *Proc. 28th Wireless Opt. Commun. Conf.*, Beijing, China, 2019, pp. 1–5.

[31] C. Li *et al.*, "Measurement-based wireless channel analysis and modelling for shipping environments," *IET Microw. Antennas Propag.*, vol. 14, pp. 812–820, 2020.

[32] A. Mahmood, E. Sisinni, L. Guntupalli, R. Rondón, S. A. Hassan, and M. Gidlund, "Scalability analysis of a LoRa network under imperfect orthogonality," *IEEE Trans. Ind. Informat.*, vol. 15, no. 3, pp. 1425–1436, Mar. 2019.

[33] *Satellite Earth Stations (SES); Possible European Standardisation of Certain Aspects of Satellite Personal Communications Networks (S-PCN) Phase 1 Report*, ETR 093, 1993

[34] C. Goursaud and Y. Mo, "Random unslotted time-frequency ALOHA: Theory and application to IoT UNB networks," in *Proc. 23rd Int. Conf. Telecommun.*, Thessaloniki, Greece, 2016, pp. 1–5.

[35] J. Kim, C. Yang, and J. S. Jang, "Performance analysis of low-Earth-orbit (LEO) mobile-satellite system using moment-based approximation of degradation factors," *IEEE Trans. Veh. Technol.*, vol. 55, no. 3, pp. 876–886, May 2006.

[36] J. M. Marais, A. M. Abu-Mahfouz, and G. P. Hancke, "A survey on the viability of confirmed traffic in a LoRaWAN," *IEEE Access*, vol. 8, pp. 9296–9311, 2020, doi: 10.1109/ACCESS.2020.2964909.

[37] A. Pop, U. Raza, P. Kulkarni, and M. Sooriyabandara, "Does bidirectional traffic do more harm than good in LoRaWAN based LPWA networks?," in *Proc. IEEE Global Commun. Conf.*, 2017, pp. 1–6.

[38] J. Markkula, K. Mikhaylov, and J. Haapola, "Simulating LoRaWAN: On importance of inter spreading factor interference and collision effect," in *Proc. IEEE Int. Conf. Commun.*, 2019, pp. 1–7

[39] M. AsadUllah, GitHub. Accessed: Sep. 10, 2021. [Online]. Available: https://github.com/MuhammadAsadUllah1/LoRaWAN-and-LEO-Satellite-Integration-for-Offshore-WindFarms-Monitoring.git

Muhammad Asad Ullah (Student Member, IEEE) received the B.S. degree in electrical engineering from the National University of Computer and Emerging Sciences, Lahore, Pakistan, in 2017, and the master's degree in wireless communications engineering in 2020 from the Centre for Wireless Communications, University of Oulu, Oulu, Finland, where he is currently working toward the Ph.D. degree in communications engineering.

His technical research interests include massive machine-type connectivity, LoRaWAN, nonterrestrial networks, and geospatial analytics.

Konstantin Mikhaylov (Senior Member, IEEE) received the B.Sc. and M.Sc. degrees in engineering from Saint-Petersburg State Polytechnical University, Saint-Petersburg, Russian Federation, in 2006 and 2008, respectively, and the Ph.D. degree in science technology from the University of Oulu, Oulu, Finland, in 2018.

He is currently an Assistant Professor for Convergent Internet of Things (IoT) Communications for Vertical Systems with the Centre for Wireless Communications, University of Oulu. He has authored or coauthored about 100 research contributions on wireless connectivity for the IoT, system design, and applications. His research interests include radio access and beyond-access technologies for massive and dependable IoT and the matters related to the design and performance of IoT devices and systems.

Hirley Alves (Member, IEEE) received the B.Sc. and M.Sc. degrees in electrical engineering from the Federal University of Technology-Paraná (UTFPR), Brazil, in 2010 and 2011, respectively, and the dual D.Sc. degree from the University of Oulu, Oulu, Finland and UTFPR, in 2015.

He is currently an Assistant Professor and the Head of the Machine-Type Wireless Communications Group, 6G Flagship, Centre for Wireless Communications, University of Oulu. His research interests include massive connectivity and ultrareliable low-latency communications for future wireless networks, 5G and 6G, and full-duplex communications.

Dr. Alves was the recipient of several awards and has been the Organizer, Chair, Technical Program Committee Member, and Tutorial Lecturer for several renowned international conferences. He is the General Chair of the 2019 International Symposium on Wireless Communication Systems (ISWCS) and the General Co-Chair of the 1st 6G Summit, Levi, Finland, in 2019, and ISWCS 2021, and the Track Chair of the 2021 IEEE International Symposium on Personal, Indoor, and Mobile Radio Communications.